JOC The Journal of Organic Chemistry

Article

pubs.acs.org/joc

Viridicatumtoxins: Expanding on a Rare Tetracycline Antibiotic Scaffold

Zhuo Shang,[†] Angela A. Salim,[†] Zeinab Khalil,[†] Michelle Quezada,[†] Paul V. Bernhardt,[‡] and Robert J. Capon*[,†]

[†]Institute for Molecular Bioscience and [‡]School of Chemistry and Molecular Biosciences, The University of Queensland, St. Lucia, Queensland 4072, Australia

Supporting Information

ABSTRACT: Viridicatumtoxins, which belong to a rare class of fungal tetracycline-like mycotoxins, were subjected to comprehensive spectroscopic and chemical analysis, leading to reassignment/assignment of absolute configurations and characterization of a remarkably acid-stable antibiotic scaffold. Structure activity relationship studies revealed exceptional growth inhibitory activity against vancomycin-resistant *Enterococci* (IC_{50} 40 nM), >270-fold more potent than the commercial antibiotic oxytetracycline.

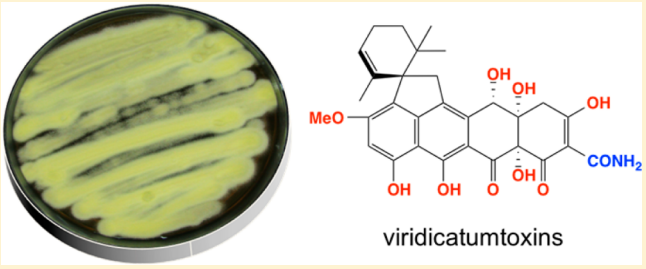

INTRODUCTION

Multidrug resistant (MDR) infectious diseases represent an extremely serious threat to modern healthcare, impacting the lives of people and communities across the world. As current and emerging mechanisms for MDR render existing antibiotics less effective, the need to develop new and improved antibiotics is becoming ever more urgent. One promising approach is to explore rare classes of microbial metabolites, first recognized but not developed as commercial antibiotics mid to late last century. Our investigations into the secondary metabolism of Australian marine-derived microbes provided an ideal platform from which to embark on such an exploration, delivering access to a wealth of bacterial and fungal strains rich in rare and novel metabolites, many with promising antibiotic properties.

In this report, we describe a comprehensive exploration of the viridicatumtoxin scaffold, a rare class of fungal polyketides closely related to the tetracycline antibiotics. Tetracyclines have been at the forefront in treating infectious diseases for over 60 years, with first generation tetracycline antibiotics (e.g., chlortetracycline, tetracycline, and oxytetracycline) inspiring second (e.g., minocycline and doxycycline) and third (e.g., tigecycline and eravacycline) generation variants, many in use today. Notwithstanding the considerable academic and industry investment in the tetracyclines over many decades, and the role they continue to play in modern healthcare, even this remarkably successful antibiotic pharmacophore is in need of renewal. We hypothesized that a better understanding of the chemical and antibiotic properties of their fungal-metabolite cousins, the viridicatumtoxins, would inform the future development of new and improved tetracycline antibiotics.

RESULTS AND DISCUSSION

An agar plate (PYGA) cultivation of a *Paecilomyces* sp. (CMB-MF010), isolated from the inner tissues of an intertidal pulmonate mollusk (*Siphonaria* sp.) collected near Shorncliffe, Queensland, Australia, exhibited promising Gram-positive antibacterial properties. Fractionation of a scaled up cultivation yielded viridicatumtoxins A (**1**)[1] and B (**2**)[2−4] and the new viridicatumtoxins D−F (**4**−**6**). Subsequent fractionation of a rice solid-phase cultivation added to this diversity, yielding all other known members of this structure class, spirohexaline (**7**)[5] and previridicatumtoxin (**8**),[6,7] together with the new viridicatumtoxin C (**3**). In this report, we present a comprehensive study of **1**−**8**, inclusive of detailed spectroscopic analysis leading to structure elucidation, assignment/reassignment of absolute configurations, inclusive of commentary on biosynthetic relationships and chemical stability, as well as antibiotic and cytotoxic properties.

HRESI(+)MS analysis of **1** and **2** revealed pseudomolecular ions consistent with the molecular formula $C_{30}H_{31}NO_{10}$ (Δmmu −0.4) and $C_{30}H_{29}NO_{10}$ (Δmmu −0.2), which detailed analysis of the 1D and 2D NMR ($CDCl_3$) data attributed to the rare fungal polyketides viridicatumtoxin[1] and viridicatumtoxin B.[2−4] Viridicatumtoxin was first described in 1973 by Hutchison et al. as a mycotoxin produced by maize meal cultures of *Penicillium viridicatum*.[1] Subsequent X-ray analyses permitted assignment of first its relative stereochemistry[8] then subsequently its absolute structure.[9] Further studies explored its biosynthesis.[6,7,10−12] Viridicatumtoxin B was reported in 2008 by Kim et al. as a co-metabolite with viridicatumtoxin from a Korean soil *Penicillium* sp. (FR11), with both metabolites exhibiting anti-MRSA activity.[2] A 2013 synthesis by Nicolaou et al. revised the structure for viridicatumtoxin B (relative configuration only) including the crystal structure of its synthetic racemate and saw viridicatumtoxin renamed viridicatumtoxin A.[3,4] In 2013 Tomoda et al.

Received: October 12, 2015
Published: November 25, 2015

DOI: 10.1021/acs.joc.5b02367
J. Org. Chem. 2015, 80, 12501−12508

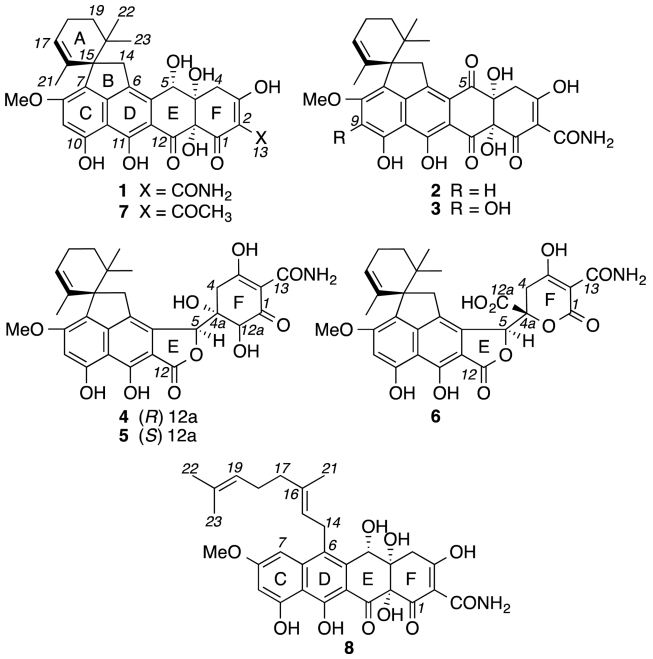

Figure 1. *Paecilomyces* sp. (CMB-MF010) viridicatumtoxins **1**–**8**.

described spirohexaline (**7**) as a co-metabolite with a purported (+)-enantiomer of viridicatumtoxin A from a rice-based cultivation of *Penicillium brasilianum* (FKI-3368).[5]

Although (+)-**1** isolated from *Paecilomyces* sp. (CMB-MF010) correlated with the (+)-enantiomer encountered by Tomoda et al.,[5] this enantiomeric configuration was contradicted by our independent X-ray analysis which is essentially the same as that reported by Silverton et al.[9] The crystal structure of **1** (isomorphous with the previously published structures of the dimethanol solvate)[8,9] was found to be the dimethanol hemihydrate. The absolute structure was confirmed by statistical analysis of anomalous dispersion effects of 2045 Bijvoet pairs collected from an entire sphere of data with Cu-Kα radiation (see Supporting Information (SI)). The absolute configurations at all four chirotopic C atoms (C-4a, C-5, C-12a, and C-15) are *S*. To explain this contradiction we speculated that viridicatumtoxin A can exist as (+)-acid and (−)-salt forms with $[\alpha]_D$ measurements of opposite sign and comparable magnitude. Consistent with this hypothesis, the (+)-acid form of **1** ($[\alpha]_D$ +31.8, EtOH) isolated from CMB-MF010 in the presence of TFA was treated with $MgSO_4$ to yield a Mg (−)-salt form ($[\alpha]_D$ −10.0, EtOH). As predicted, on exposure to HCl the (−)-salt reverted to the (+)-acid. Significantly, a commercial sample of viridicatumtoxin A was determined to be a (−)-salt, with HCl treatment leading to conversion to the (+)-acid. Comparable changes in the $[\alpha]_D$ of **1** and oxytetracycline (**9**) were also observed in a range of solvents, suggesting that this differential acid/salt optical rotation phenomenon is a characteristic of the tetracycline scaffold. Based on these observations and on consideration of published isolation protocols, we propose that the (+)-enantiomers of viridicatumtoxins A and B reported by Tomoda et al.[5] and Kim et al.,[2] respectively, are in fact the free acids (+)-**1** and (+)-**2**, respectively, as isolated and characterized herein.

Furthermore, with detailed spectroscopic analysis identifying **7** ($C_{31}H_{32}O_{10}$, Δmmu +0.1) as spirohexaline,[5] on biosynthetic grounds we take this opportunity to correct its absolute configuration, aligning it with the co-metabolite **1** (Figure 1). Likewise, spectroscopic analysis identified **8** ($C_{30}H_{33}NO_{10}$, Δmmu −0.3) as previridicatumtoxin, first reported in 2012 as a late-stage biosynthetic precursor to **1** accumulated in the gene deletion strain *Penicillium aethiopicum* Δ*gsfA*,[6,7] we now acknowl-

Table 1. ^{1}H NMR (600 MHz) Data for Viridicatumtoxins C–F (3–6)

pos.	3[a]	4[b]	5[b]	6[b]
4	α 2.83 (d, 18.6)	α 2.44 (d, 17.6)	α 2.39 (d, 18.3)	α 3.15 (d, 17.2)
	β 3.08 (d, 18.6)	β 2.02 (d, 17.6)	β 2.66 (d, 18.3)	β 2.98 (d, 17.2)
5	–	5.65 (s)	5.72 (s)	5.85 (s)
9	–	6.61 (s)	6.60 (s)	6.60 (s)
12a	–	4.53 (br s)	4.29 (br s)	–
14	α 4.00 (d, 19.8)	α 3.19 (d, 18.1)	α 3.25 (d, 17.6)	α 3.20 (d, 17.5)
	β 3.14 (d, 19.8)	β 3.09 (dd, 18.1, 1.6)	β 3.09 (d, 17.6)	β 2.92 (d, 17.5)
17	5.58 (br s)	5.37 (br s)	5.42 (br s)	5.39 (br s)
18	α 2.13 (m)	α 1.92 (br d, 18.0)	α 1.95 (br d, 18.4)	α 1.91 (br d, 18.6)
	β 2.23 (m)	β 2.14 (m)	β 2.17 (m)	β 2.15 (m)
19	1.71 (m)	α 1.74 (m)	α 1.78 (m)	α 1.76 (m)
	–	β 1.25 (dd, 13.0, 5.9)	β 1.27 (dd, 13.3, 5.7)	β 1.25 (dd, 13.1, 5.8)
21	1.45 (s)	1.47 (s)	1.51 (s)	1.46 (s)
22	0.88 (s)	0.85 (s)	0.85 (s)	0.81 (s)
23	0.63 (s)	0.34 (s)	0.33 (s)	0.30 (s)
8-OCH_3	4.05 (s)	3.80 (s)	3.80 (s)	3.78 (s)
3-OH	17.91 (br s)	–	–	–
4a-OH	4.23 (br s)	–	–	–
9-OH	5.97 (br s)[c]	–	–	–
10-OH	8.44 (br s)	–	–	–
11-OH	14.14 (br s)	–	–	–
12a-OH	4.89 (br s)	–	–	–
13-NH_2	a 9.21 (br s)	–	–	–
	b 5.97 (br s)[c]	–	–	–

[a] ^{1}H NMR spectra were acquired in $CDCl_3$. [b] ^{1}H NMR spectra were acquired in $CDCl_3/CD_3OD$ (4:1).; [c] Overlapping signals.

DOI: 10.1021/acs.joc.5b02367
J. Org. Chem. 2015, 80, 12501–12508

Table 2. ^{13}C NMR (150 MHz) Data for Viridicatumtoxins A−F (1−6), Spirohexaline (7), and Previridicatumtoxin (8)

pos.	1[a]	2[a]	3[a]	4[b]	5[b]	6[b]	7[a]	8[a]
1	190.6	194.3	193.6	194.5	192.8	166.2	190.3	190.1
2	99.7	99.7	99.7	99.2	99.4	99.1	110.6	99.6
3	192.9	192.8	192.9	192.7	191.3	189.7	194.5	193.0
4	40.5	42.2	42.4	36.8	39.0	35.9	40.8	40.4
4a	71.6	77.8	77.3	76.0	75.9	81.3	71.3	71.3
5	71.8	188.8	188.7	80.2	81.2	80.5	71.7	71.3
5a	137.2	146.4[c]	145.6[c]	130.5	130.2	129.5	137.3	130.5
6	123.9	124.9[c]	133.0[c]	130.0	129.4	128.7	123.8	130.8
6a	147.3	144.8[c]	137.5[c]	148.7	148.1	148.5	147.3	140.9
7	122.8	127.3	114.9	121.9	121.3	121.7	122.8	99.9
8	160.9	161.3	150.4	157.8	157.6	157.8	160.9	164.8
9	100.0	102.6	140.3	98.9	99.0	99.1	100.0	102.2
10	158.1	158.4	141.6	155.8	155.3	155.9	158.1	161.1
10a	105.6	106.9	108.5	107.2	106.2	107.3	105.6	108.7
11	166.1	165.4	162.3	171.3	170.7	170.5	166.1	167.2
11a	105.2	107.3	108.6	103.6	102.4	103.4	105.2	104.2
12	195.3	195.2	196.6	155.0	153.5	154.8	195.4	195.7
12a	80.3	80.7	80.8	74.3	77.8	170.3	80.8	79.4
13	172.8	173.0	173.0	172.8	172.0	172.7	202.4	172.8
14	41.3	44.6	43.4	43.8	43.0	42.0	41.3	27.3
15	60.2	60.6	61.4	60.0	59.5	60.2	60.2	122.3
16	136.7	135.8	135.1	137.5	137.0	137.3	136.7	137.0
17	121.5	122.0	122.8	120.7	120.4	121.0	121.5	39.7
18	23.0	23.0	23.0	23.0	22.5	22.9	23.0	26.7
19	34.0	34.2	34.3	34.0	33.5	33.8	34.0	123.9
20	38.7	38.5	37.9	38.3	37.9	38.3	38.7	131.9
21	21.1	20.9	20.8	21.3	20.8	21.0	21.1	16.7
22	24.1	24.5	25.2	23.9	23.4	23.7	24.1	25.8
23	25.6	25.6	25.7	25.6	25.1	25.5	25.6	17.9
2-$COCH_3$	–	–	–	–	–	–	27.9	–
8-OCH_3	55.7	55.8	60.7	55.5	55.1	55.4	55.7	55.7

[a]^{13}C NMR spectra were acquired in $CDCl_3$. [b]^{13}C NMR spectra were acquired in $CDCl_3$/CD_3OD (4:1). [c]The chemical shifts of carbons were tentatively assigned by ACD simulation.

edge **8** as a natural product with an absolute configuration in common with its co-metabolite **1**. Having fully characterized and assigned/corrected absolute configurations for all four known viridicatumtoxins (**1**−**2**, **7**−**8**), we now describe the new viridicatumtoxins C−F (**3**−**6**).

HRESI(+)MS analysis of **3** returned a molecular formula ($C_{30}H_{29}NO_{11}$, Δmmu −0.1) consistent with an oxygenated homologue of **2**. Comparison of the ^{1}H NMR ($CDCl_3$) data for **3** (Table 1) with those of **2** revealed the only significant differences as replacement of H-9 (δ_H 6.80) in **2** with a phenolic hydroxyl (δ_H 5.97) in **3** and a deshielding of 8-OMe (δ_H 3.90 to δ_H 4.05). Analysis of the ^{13}C NMR data (Table 2) revealed substitution of the C-9 methine in **2** (δ_C 102.6) with a phenolic moiety in **3** (δ_C 140.3), the latter featuring an HMBC correlation to 10-OH (δ_H 8.44). These observations, together with diagnostic 2D NMR correlations (Figure 2), permitted assignment of the structure for viridicatumtoxin C (**3**) as indicated, with the absolute configuration assigned on the basis of biosynthetic links to **1**. Supportive of this assignment, analytical scale treatment of **3** with acid or heat resulted in oxidative conversion to an *ortho*-quinone (**3a**), as evidenced by conversion to an *ortho*-phenylenediamine adduct (**3b**) (Figures 2 and S3).

HRESI(+)MS analysis of **4** returned a molecular formula ($C_{30}H_{31}NO_{10}$, Δmmu +0.2) isomeric with **1**. Comparison of the 1D NMR ($CDCl_3$:MeOH-d_4 [4:1]) data for **4** (Tables 1−2) with **1**, together with diagnostic 2D NMR correlations (Figure 3), confirmed common ring A-D and ring F (C-1 to C-4) substructures. Further comparisons revealed the oxymethine resonances for H-5/C-5 in **4** (δ_H 5.65; δ_C 80.2) were significantly deshielded compared to **1** (δ_H 4.50; δ_C 71.8), with **1** and **4** exhibiting common HMBC correlations from H-5 to C-4, C-4a, C-5a, C-6, C-11a, and C-12a and with the quaternary C-12a (δ_C

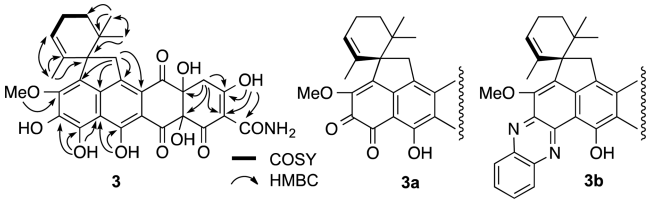

Figure 2. Diagnostic 2D NMR correlations for **3** and derivatives **3a**−**b**.

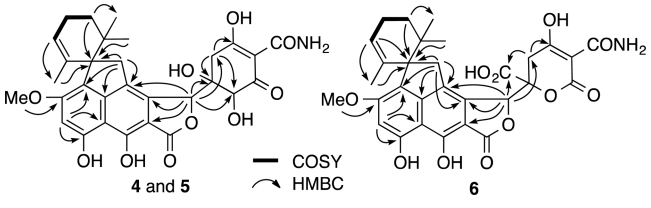

Figure 3. Diagnostic 2D NMR correlations for **4**, **5**, and **6**.

DOI: 10.1021/acs.joc.5b02367
J. Org. Chem. 2015, 80, 12501−12508

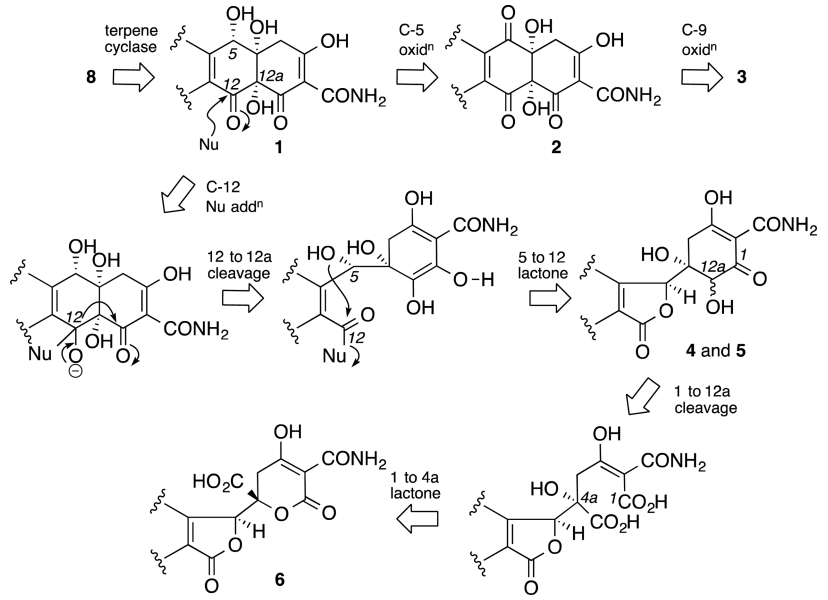

Figure 4. Plausible biosynthetic pathway linking **1** with **2**–**6** and **8**.

80.3) and C-12 (δ_C 195.3) in **1** replaced by oxymethine (δ_H 4.53; δ_C 74.3) and ester/lactone (δ_C 155.0) resonances in **4**. As further evidence of a C-12a secondary OH moiety, a sample of **4** was converted to the tetraacetate **4a** (Figure S28) to reveal the predicted deshielding of the H-12a methine (**4** δ_H 4.53; **4a** δ_H 5.74).

Based on these observations we propose that **4** is a *seco*-ring E analogue of **1**, formed by nucleophilic attack at C-12, leading to cleavage of the C-12 to C-12a bond and subsequent intramolecular lactonisation from 5-OH to C-12 (Figure 4). We anticipate that this sequence proceeds with retention of configuration about C-15, C-4a, and C-5 and racemization about C-12a. Consistent with this hypothesis, viridicatumtoxin E (**5**) was identified as the C-12a epimer of **4**, with individual C-12a configurations inferred from ROESY correlations (Table S11). Diagnostic ROESY correlations (Figures 5 and S41–S42)

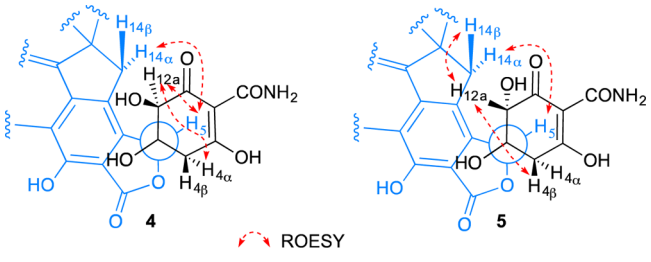

Figure 5. Diagnostic ROESY correlations for **4** and **5**.

established *syn* relationships between $H_{4\alpha}/H_{12a}$ in **4** and $H_{4\beta}/H_{12a}$ in **5**, with both **4** and **5** possessing a common H_5 to $H_{14\alpha}$ configuration. Significantly, a key ROESY correlation positioned H_{12a} and $H_{14\beta}$ in close proximity in **5** (C_{12a} *S*), necessitating an epimeric configuration for **4** (C_{12a} *R*).

HRESI(+)MS analysis of **6** returned a molecular formula ($C_{30}H_{29}NO_{11}$, Δmmu +0.2) suggestive of an oxidized analogue of **4** (and **5**). Comparison of 1D and 2D NMR ($CDCl_3$:MeOH-d_4 [4:1]) (Tables 1–2) data for **6** with **4** revealed common rings A-E and C-2 to C-4 ring F substructures (Figure 1), with 1D NMR differences focused around replacement of the C-12a/H-12a oxymethine (δ_C 74.3; δ_H 4.53) and C-1 ketone (δ_C 194.5) in **4** with a C-12a carboxylic acid (δ_C 170.3) and C-1 ester/lactone (δ_C 166.2) in **6** and a deshielding of H_2-4 ($\Delta\delta_H$ 0.71 and 0.96) and C-4a ($\Delta\delta_C$ 5.3) in **6** compared to **4**. Diagnostic 2D HMBC correlations (Figure 3) positioned the carboxylic acid moiety at C-4a, necessitating closure of a C-1 to C-4a lactone, and permitting assignment of the planar structure as indicated. A plausible biosynthetic pathway (Figure 4) provides an alternate oxidative C-1 to C-12a cleavage of the precursor linking **1** with **4** and **5**, to deliver viridicatumtoxin F (**6**), with conservation of configuration about all chiral centers.

Viridicatumtoxins D (**4**) and E (**5**) bear a striking structural similarity to α-apo-oxytetracycline (**11**) and β-apo-oxytetracycline (**12**), well-known but poorly characterized acid degradation products and impurities detected in the commercial antibiotic oxytetracycline (**9**).[13] To support structure assignments for **4** and **5**, we subjected **9** to two acid degradation protocols: (i) 1 h at 75 °C in 0.1 M HCl_{aq} (pH 1), and (ii) 4 h at 37 °C in 0.01 M HCl_{aq} (pH 2), to yield authentic standards of **11** and **12** together with the associated artifacts **10** and **13** (Figures 6 and S7–S8). Structures for **11**–**13** were confirmed by detailed spectroscopic analysis (Tables S17–S19). By contrast, extended treatment of **1** under these conditions (>10 h) resulted in no degradation (Figure S6), with the more forcing conditions of 20 h at 100 °C in

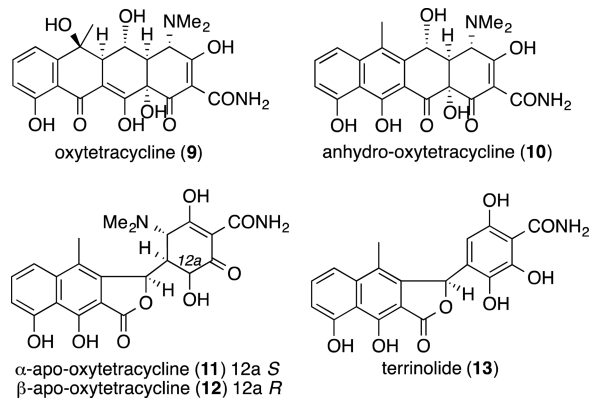

Figure 6. Oxytetracycline (**9**) and degradation products **10**–**13**.

DOI: 10.1021/acs.joc.5b02367
J. Org. Chem. 2015, 80, 12501–12508

5% *p*-toluene sulfonic acid/toluene delivering very minor yields (~1.5%) of the quinone-methides **14** ($C_{28}H_{28}O_7$, Δmmu −0.3) and **15** ($C_{27}H_{24}O_6$, Δmmu −0.5) (Figures 7 and S9). Our studies reveal for the first time that viridicatumtoxin A is remarkably acid stable, in stark contrast to the highly acid labile tetracycline framework, confirming **4**−**6** as natural products not handling artifacts.

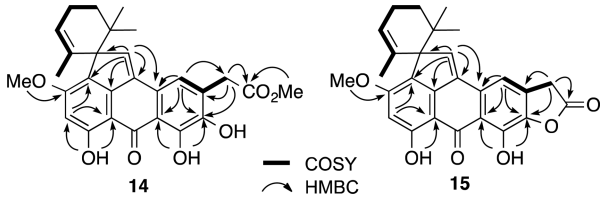

Figure 7. Viridicatumtoxin A (**1**) minor degradation products **14**−**15**.

Although originally described as a mycotoxin,[1] oral dosage of **1** has been judged non-toxic to mice (up to 350 mg/kg) and rats (up to 150 mg/kg).[14] Armed with a comprehensive suite of all known and new viridicatumtoxins (**1**−**8**), we compared their growth inhibitory properties against a panel of drug-resistant Gram-positive and -negative bacteria with those of the tetracycline antibiotic **9** and its acid degradation products **11**−**13** (Table S4). While **1**−**5** and **7**−**8** exhibited anti-MRSA properties comparable with **9**, viridicatumtoxin B (**2**) was especially effective against VRE, with an IC_{50} > 270-fold more potent than **9**, albeit with moderate levels of cytotoxicity against three human cancer cell lines (Table 3).

Table 3. Antibacterial and Cytotoxicity Properties (IC_{50} μM) of 1−9 and 11−13

	MRSA-2[a]	VRE[b]	NCI-H460[c]	KB3-1[d]	SW620[e]
1	1.2	1.1	1.0	2.5	1.0
2	0.15	0.04	0.6	1.6	0.6
3	1.7	1.5	9.2	11.0	17.4
4	9.7	3.4	24.2	>30	20.7
5	3.3	1.5	>30	>30	>30
6	>30	>30	>30	>30	>30
7	2.3	3.1	11.3	6.3	16.7
8	4.4	4.8	5.3	4.1	6.0
9	0.5	11.0	15.9	21.3	>30
11	>30	>30	>30	>30	>30
12	>30	>30	>30	>30	>30
13	>30	>30	>30	>30	>30

[a]AUS-RBWH-MRSA-02 (methicillin-resistant *Staphylococcus aureus*). [b]AUS-RBWH-VRE-01 (vancomycin-resistant *Enterococcus faecalis*). [c]NCI-H460 is a human lung carcinoma cell line. [d]KB3-1 is a human cervix carcinoma cell line. [e]SW620 is a human colon carcinoma cell line.

Knowledge of the acid-stable viridicatumtoxin scaffold informs our ability to increase the acid stability of the tetracycline antibiotics, which are easily degraded into the non-active analogues when taken orally. Possible modifications to the tetracycline framework include deamination at C-4, oxidation at C-4a and C-5, dehydration across C-5a and C-6, alkylation at C-6 and C-7, and oxidation at C-8 (Figure 8).

In conclusion, our investigations into the chemistry of the marine mollusk-derived *Paecilomyces* sp. (CMB-MF010) have greatly expanded knowledge of the viridicatumtoxins, a rare family of mycotoxins closely related to the tetracycline class of

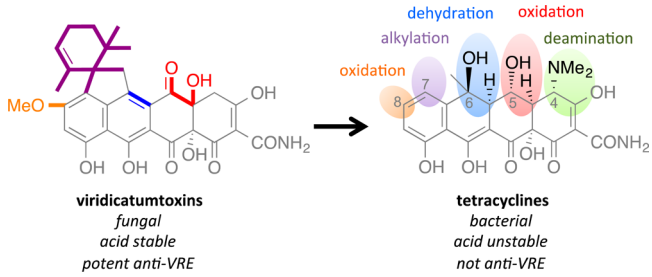

Figure 8. Viridicatumtoxin inspired modifications to tetracyclines.

antibiotics. In the course of our studies, we documented the exceptional acid stability of the viridicatumtoxins, with co-metabolite inspired structure activity relationship investigations revealing the 5-oxo analogue, viridicatumtoxin B (**2**), as a potent vancomycin-resistant *Enterococci* (VRE) antibiotic. Knowledge acquired during our investigations has the potential to inform the redesign of the tetracycline framework, enhancing acid stability and oral bioavailability, while simultaneously optimizing for and extending antibiotic efficacy to include therapeutically challenging pathogens such as VRE.

EXPERIMENTAL SECTION

General Experimental Details. Specific optical rotations ($[\alpha]_D$) were acquired on a polarimeter in a 100 × 2 mm cell at room temperature. UV−vis spectra were obtained on a UV−vis spectrophotometer with 1 cm quartz cells. Circular dichroism (CD) spectra were recorded on a spectropolarimeter in 1 mm quartz cells at room temperature with scanning speed of 50 nm/min and 0.5 nm step scan over the wavelength from 200−600 nm. Nuclear magnetic resonance (NMR) spectra were acquired on a 600 MHz spectrometer with either a 5 mm PASEL 1H/D-13C Z-gradient probe or 5 mm CPTCI 1H/19F-13C/15N/DZ-gradient cryoprobe. In all cases spectra were acquired at 25 °C (unless otherwise specified) in solvents as specified in the text, with referencing to residual ^1H or ^{13}C signals in the deuterated solvents. Electrospray ionization mass spectrometry (ESIMS) experiments were carried out on a LC/MSD (quadrupole) instrument in both positive and negative modes. High-resolution ESIMS spectra were obtained on a micrOTOF mass spectrometer either by direct injection in MeCN at 3 μL/min using sodium formate clusters as an internal calibrant or by hyphenating with LC system comprising of corresponding pump, column compartment, autosampler, photodiode array (PDA) detector.

Collection and Isolation of *Paecilomyces* sp. (CMB-MF010). The fungus CMB-MF010 was isolated in 2012 from the inner tissue of a marine pulmonate false limpet *Siphonaria* sp. collected at the rocky intertidal zone of Moora Park, Shorncliffe, Queensland. The fresh *Siphonaria* sample was transported in a sterile tube (50 mL) on ice to the laboratory, where it was rinsed in sterile natural seawater for 1 min and subjected to surface sterilization in 70% ethanol (v/v) for 30 s, after which it was washed with sterile seawater to remove traces of EtOH. Subsequently, the sample was dissected under aseptic conditions, and the inner tissue placed on PYG agar plates (comprising 2% glucose, 1% peptone, 0.5% yeast extract, 0.02% chloramphenicol, and 1.5% agar in 50% artificial seawater (1.7% salinity)). The plates were wrapped in parafilm and incubated at 26.5 °C for 3−4 weeks. A pure culture of fungus CMB-MF010 was obtained by single-colony serial transfer on agar plates and then cryopreserved at −80 °C in 15% aqueous glycerol. Taxonomic analysis identified CMB-MF010 as a *Paecilomyces* sp. (see SI).

Analytical Cultivation and Chemical Profiling of *Paecilomyces* sp. (CMB-MF010). *Paecilomyces* sp. (CMB-MF010) was screened in PSB broth (1% sucrose, 1% mannitol, 0.5% peptone, 0.3% yeast extract, and 20% potato juice in water; 200 rpm at 26.5 °C for 7 d in microbioreactor), on PYG agar plates (2% glucose, 1% peptone, 0.5% yeast extract, and 1.5% agar; 26.5 °C for 25 d) with and without natural sea salts and on rice solid medium (70 g rice, 0.3% peptone, 0.3% yeast extract, 0.1% monosodium glutamate, and 1.7 g natural sea salt prepared

DOI: 10.1021/acs.joc.5b02367
J. Org. Chem. 2015, 80, 12501−12508

in 100 mL distilled water; 26 °C for 25 d). After cultivation, the broth and solid matrix were extracted exhaustedly with EtOAc, and the organic phase was dried in vacuo to yield crude extracts. Analytes of crude extracts (5 mg/mL) were prepared in MeOH for HPLC-DAD-ESI(±)MS analysis by standard gradient elution (Zorbax SB-C_8 column, 150 × 4.6 mm, 5 μm, 1 mL/min gradient elution from 90% H_2O/MeCN to 100% MeCN with 0.05% formic acid in MeCN as modifier over 15 min). The fungus CMB-MF010 produced different secondary metabolites when grown on PYG agar and rice solid media (Figure S1).

Preparative Cultivation and Fractionation of *Paecilomyces* sp. (CMB-MF010). A single colony of *Paecilomyces* sp. (CMB-MF010) was subsampled on PYG agar plates (×100) (2% glucose, 1% peptone, and 0.5% yeast extract, prepared in distilled water) and incubated at 26.5 °C for 25 days. The resulting agar plates were harvested, diced (~1 cm^3), and extracted with EtOAc until the organic phase was almost colorless. The combined organic phase was concentrated in vacuo to yield a crude extract (1173 mg), which was sequentially triturated to afford hexane (153.9 mg), CH_2Cl_2 (700.0 mg), and MeOH (144.0 mg) soluble partitions. The CH_2Cl_2 solubles were subjected to SPE chromatography (GracePure C_{18}-Max with a 10% stepwise gradient elution from 70% H_2O/MeOH to MeOH), and the peaks of interest (HPLC-DAD-MS) concentrated in two fractions. The first fraction (38.7 mg) was fractionated with HPLC (Zorbax SB-C_8 column, 250 × 9.4 mm, 5 μm, 3 mL/min gradient elution from 65% to 48% H_2O/MeCN over 5 min, followed by 48% to 43% H_2O/MeCN over 10 min, with a constant 0.01% TFA/MeCN modifier) to yield viridicatumtoxin D (**4**) (t_R = 12.4 min; 8.2 mg, 0.7%), viridicatumtoxin E (**5**) (t_R = 11.8 min; 7.5 mg, 0.6%), and viridicatumtoxin F (**6**) (t_R = 11.2 min; 2.6 mg, 0.2%). The second fraction (96.3 mg) was fractionated by HPLC (Zorbax SB-C_8 column, 250 × 9.4 mm, 5 μm, 3 mL/min gradient elution from 65% to 48% H_2O/MeCN over 5 min, followed by 48% to 43% H_2O/MeCN over 10 min, and from 43% to 30% H_2O/MeCN over 5 min, with a constant 0.01% TFA/MeCN modifier) to afford viridicatumtoxin A (**1**) (t_R = 18.9 min; 14.1 mg, 1.2%) and viridicatumtoxin B (**2**) (t_R = 20.3 min; 0.6 mg, 0.05%).

For cultivation on rice solid media, a small sample (~1 cm^3) of CMB-MF010 colony on agar was used to inoculate a 1 L Erlenmeyer flask containing sterile rice medium, and the mixture was incubated at 26 °C for 25 days. The fungal mycelia as well as the rice media were exhaustively extracted with EtOAc and concentrated in vacuo to obtain a combined EtOAc extract (673.0 mg), which was sequentially triturated to yield hexane (375.9 mg), CH_2Cl_2 (161.1 mg) and MeOH (22.1 mg) solubles, respectively. The CH_2Cl_2 solubles (161.1 mg) were subjected to C_{18} SPE fractionation (90% H_2O/MeOH to MeOH) to yield 10 fractions. After HPLC-DAD-MS analysis, the 50%, 40%, and 30% H_2O/MeOH fractions were combined (18.4 mg) and further fractionated by HPLC (Zorbax SB-C_8 column, 250 × 9.4 mm, 5 μm, 3 mL/min isocratic elution at 45% H_2O/MeCN over 20 min with a constant 0.01% TFA/MeCN modifier) to afford viridicatumtoxin A (**1**) (t_R = 13.9 min; 7.4 mg, 1.1%) and viridicatumtoxin C (**3**) (t_R = 10.5 min; 4.0 mg, 0.6%). After freeze-drying, the slightly impure viridicatumtoxin C (**3**) sample was repurified by HPLC (same elution condition as above) to yield pure viridicatumtoxin C (**3**) (t_R = 10.5 min; 2.9 mg, 0.4%) and pure *ortho*-quinone viridicatumtoxin C (**3a**) (t_R = 9.8 min; 0.6 mg). The 10% H_2O/MeOH fraction (53.0 mg) was further fractionated by HPLC (Zorbax SB-C_3 column, 250 × 9.4 mm, 5 μm, 3 mL/min gradient elution from 50% to 35% H_2O/MeCN over 15 min followed by a 5 min hold at 100% MeCN, with a constant 0.01% TFA/MeCN modifier) to yield spirohexaline (**7**) (t_R = 15.4 min; 0.3 mg, 0.04%) and previridicatumtoxin (**8**) (t_R = 15.9 min; 0.4 mg, 0.06%).

Note: % yields for compounds **1**−**8** are calculated as weight-to-weight estimate against the crude extract (1172.7 mg for agar plates and 673.0 mg for rice solid media).

Characterization of *Paecilomyces* sp. (CMB-MF010) Metabolites. *Viridicatumtoxin A (**1**).* Bright-yellow powder; $[\alpha]_D^{22}$ +31.8 (*c* 0.2, EtOH); UV (MeOH) λ_{max} (log ε) 236 (4.44), 282 (4.53), 424 (3.94) nm; CD (MeOH) λ_{max} ($\Delta\varepsilon$) 237 (−14.4), 287 (+29.4), 346.5 (−3.0), 361.5 (−0.1), 422.5 (−2.7) nm; NMR (600 MHz, $CDCl_3$) see Tables 2 and S6; ESI(+)MS *m*/*z* 548 $[M - H_2O + H]^+$, 588 $[M + Na]^+$, ESI(−)MS *m*/*z* 564 $[M - H]^-$; HRESI(+)MS *m*/*z* 588.1844 $[M + Na]^+$ (calcd for $C_{30}H_{31}NO_{10}Na^+$, 588.1840).

*Viridicatumtoxin B (**2**).* Bright-yellow powder; $[\alpha]_D^{22}$ +43.3 (*c* 0.05, EtOH); UV (MeOH) λ_{max} (log ε) 255 (4.40), 285 (4.35, sh), 431 (3.94), 455 (3.99) nm; CD (MeOH) λ_{max} ($\Delta\varepsilon$) 206.5 (−5.4), 227.5 (+4.7), 256 (−1.8), 276.5 (+17.9), 328 (−1.4), 351 (−0.3), 385 (−1.5), 421 (+0.9), 434 (−0.7), 444.5 (−0.1), 459.5 (−4.2) nm; NMR (600 MHz, $CDCl_3$) see Tables 2 and S7; ESI(+)MS *m*/*z* 564 $[M + H]^+$, 586 $[M + Na]^+$, ESI(−)MS *m*/*z* 562 $[M - H]^-$; HRESI(−)MS *m*/*z* 562.1721 $[M - H]^-$ (calcd for $C_{30}H_{28}NO_{10}$, 562.1719).

*Viridicatumtoxin C (**3**).* Yellow powder; $[\alpha]_D^{22}$ +41.1 (*c* 0.08, EtOH); UV (MeOH) λ_{max} (log ε) 257 (4.42), 303 (4.40), 448 (4.04) nm; CD (MeOH) λ_{max} ($\Delta\varepsilon$) 226 (+6.1), 251 (−6.3), 271 (+7.9), 298 (+0.2), 321.5 (+2.5) nm; NMR (600 MHz, $CDCl_3$) see Tables 1−2 and S8; ESI(+)MS *m*/*z* 580 $[M + H]^+$, 602 $[M + Na]^+$, ESI(−)MS *m*/*z* 578 $[M - H]^-$; HRESI(+)MS *m*/*z* 602.1634 $[M + Na]^+$ (calcd for $C_{30}H_{29}NO_{11}Na^+$, 602.1633).

*Viridicatumtoxin D (**4**).* Brown amorphous powder; $[\alpha]_D^{22}$ +21.7 (*c* 0.06, EtOH); UV (MeOH) λ_{max} (log ε) 263 (4.64), 344 (3.89), 396 (3.98) nm; CD (MeOH) λ_{max} ($\Delta\varepsilon$) 206 (−2.0), 225.5 (−10.7), 260 (+38.4), 279 (−6.7), 308 (−0.9), 378.5 (−2.7) nm; NMR (600 MHz, $CDCl_3/CD_3OD$ = 4:1) see Tables 1−2 and S9; ESI(+)MS *m*/*z* 566 $[M + H]^+$, ESI(−)MS *m*/*z* 564 $[M - H]^-$; HRESI(+)MS *m*/*z* 588.1838 $[M + Na]^+$ (calcd for $C_{30}H_{31}NO_{10}Na^+$, 588.1840).

*Viridicatumtoxin D Tetratacetate (**4a**).* A solution of **4** (2 mg, 3.54 μmol) in pyridine (250 μL) and acetic anhydride (200 μL) was stirred at room temperature for 30 h, after which it was dried under N_2, and the crude product subjected to HPLC fractionation (Zorbax SB-C_8 column, 250 × 9.4 mm, 5 μm, 3 mL/min gradient elution from 35% to 20% H_2O/MeCN over 15 min, with an isocratic 0.01% TFA/MeCN modifier) to yield the tetraacetate **4a** (t_R = 9.92 min; 1.5 mg, 75%) as light brown powder; UV (MeOH) λ_{max} (log ε) 268 (4.75), 347 (3.91) nm; ^{1}H NMR (600 MHz, $CDCl_3/CD_3OD$ = 4:1) δ_H 7.07 (1H, s, H-9), 5.74 (1H, s, H-12a), 5.58 (1H, s, H-5), 5.46 (1H, br s, H-17), 3.86 (3H, s, 8-OCH_3), 3.43 (1H, d, *J* = 18.6 Hz, H-14α), 3.25 (1H, d, *J* = 18.6 Hz, H-14β), 2.58 (1H, d, *J* = 17.0 Hz, H-4α), 2.45 (3H, s, $COCH_3$), 2.41 (3H, s, $COCH_3$), 2.33 (3H, s, $COCH_3$), 2.30 (3H, s, $COCH_3$), 2.19 (1H, m, H-18β), 2.05 (1H, d, *J* = 17.0 Hz, H-4β), 1.97 (1H, br d, *J* = 18.2 Hz, H-18α), 1.80 (1H, ddd, *J* = 18.4, 12.6, 6.2 Hz, H-19α), 1.52 (3H, s, H-21), 1.31 (1H, dd, *J* = 13.4, 6.2 Hz, H-19β), 0.89 (3H, s, H-22), 0.33 (3H, s, H-23); ESI(+)MS *m*/*z* 734 $[M + H]^+$, 756 $[M + Na]^+$, ESI(−)MS *m*/*z* 732 $[M - H]^-$; HRESI(+)MS *m*/*z* 756.2263 $[M + Na]^+$ (calcd for $C_{38}H_{39}NO_{14}Na^+$, 756.2263).

*Viridicatumtoxin E (**5**).* Brown amorphous powder; $[\alpha]_D^{22}$ +272.2 (*c* 0.05, EtOH); UV (MeOH) λ_{max} (log ε) 263 (4.64), 344 (3.91), 383 (3.99) nm; CD (MeOH) λ_{max} ($\Delta\varepsilon$) 211.5 (+0.9), 225.5 (−7.5), 266 (+40.6), 326 (−2.7), 360.5 (+2.1) nm; NMR (600 MHz, $CDCl_3/CD_3OD$ = 4:1) see Tables 1−2 and S10; ESI(+)MS *m*/*z* 566 $[M + H]^+$, 588 $[M + Na]^+$, ESI(−)MS *m*/*z* 564 $[M - H]^-$; HRESI(+)MS *m*/*z* 588.1840 $[M + Na]^+$ (calcd for $C_{30}H_{31}NO_{10}Na^+$, 588.1840).

*Viridicatumtoxin F (**6**).* Brown amorphous powder; $[\alpha]_D^{22}$ +146.2 (*c* 0.06, EtOH); UV (MeOH) λ_{max} (log ε) 263 (4.55), 347 (3.85), 376 (3.90) nm; CD (MeOH) λ_{max} ($\Delta\varepsilon$) 213.5 (+5.9), 247 (−5.4), 265 (+43.9), 328.5 (−1.3), 359 (+0.7) nm; NMR (600 MHz, $CDCl_3/CD_3OD$ = 4:1) see Tables 1−2 and S12; ESI(+)MS *m*/*z* 580 $[M + H]^+$, ESI(−)MS *m*/*z* 578 $[M - H]^-$, 534 $[M - CO_2 - H]^+$; HRESI(+)MS *m*/*z* 602.1631 $[M + Na]^+$ (calcd for $C_{30}H_{29}NO_{11}Na^+$, 602.1633).

*Spirohexaline (**7**).* Bright-yellow powder; $[\alpha]_D^{22}$ +15.5 (*c* 0.03, EtOH); UV (MeOH) λ_{max} (log ε) 236 (4.15), 283 (4.34), 426 (3.69) nm; NMR (600 MHz, $CDCl_3$) see Tables 2 and S13; ESI(+)MS *m*/*z* 547 $[M - H_2O + H]^+$, 587 $[M + Na]^+$, ESI(−)MS *m*/*z* 563 $[M - H]^-$; HRESI(−)MS *m*/*z* 563.1922 $[M - H]^-$ (calcd for $C_{31}H_{31}O_{10}$, 563.1923).

*Previridicatumtoxin (**8**).* Bright-yellow powder; $[\alpha]_D^{22}$ +98.8 (*c* 0.04, EtOH); UV (MeOH) λ_{max} (log ε) 241 (4.50), 273 (4.65), 415 (4.15) nm; NMR (600 MHz, $CDCl_3$) see Tables 2 and S14; ESI(+)MS *m*/*z* 550 $[M - H_2O + H]^+$, 568 $[M + H]^+$, 590 $[M + Na]^+$, ESI(−)MS *m*/*z* 566 $[M - H]^-$; HRESI(−)MS *m*/*z* 566.2035 $[M - H]^-$ (calcd for $C_{30}H_{32}NO_{10}$, 566.2032).

Oxidation and Derivatization of Viridicatumtoxin C (3). A mixture sample of **3** (65%, w/w) and **3a** (35%, w/w) in MeOH (40 μL) was heated at 40 °C overnight, and the product dried under N_2,

DOI: 10.1021/acs.joc.5b02367
J. Org. Chem. 2015, 80, 12501−12508

redissolved in MeOH (20 μL), and subjected to HPLC-DAD-MS analysis (Zorbax SB-C_8 column, 150 × 4.6 mm, 5 μm, 1 mL/min gradient elution from 90% H_2O/MeCN to 100% MeCN with 0.05% formic acid as modifier over 15 min) to detect the significant transformation of viridicatumtoxin C (**3**) to *ortho*-quinone viridicatumtoxin C (**3a**) (90%, w/w); UV (MeOH) λ_{max} (log ε) 265 (4.48), 468 (3.65), 591 (3.72) nm; ESI(+)MS m/z 578 $[M + H]^+$, ESI(−)MS m/z 576 $[M - H]^-$; HRESI(+)MS m/z 600.1481 $[M + Na]^+$ (calcd for $C_{30}H_{27}NO_{11}Na^+$, 600.1476). To confirm the structure, **3a** was treated with 1,2-phenylenediamine (PLDA) and analyzed by HPLC-DAD-HRMS (Gemini-NX C_{18} column, 150 × 2.0 mm, 5 μm, 250 μL/min gradient elution from 90% H_2O/MeCN to 100% MeCN (with isocratic 0.05% formic acid as modifier) over 10 min at 35 °C, then held for 5 min and equilibrated for 4 min; 100 μL/h injection of sodium formate clusters as an internal calibrant) to detect 95% conversion to the adduct **3b**; $C_{36}H_{31}N_3O_9$ m/z 650.2098 $[M + H]^+$ (calcd for $C_{36}H_{32}N_3O_9^+$, 650.2133) (Figure S3).

Acid Stability of Viridicatumtoxin A (1) and Oxytetracycline (9). Experiment 1: Individual aliquots of **1** (100 μg) and **9** (100 μg) were treated with 0.1 M HCl (200 μL, pH = 1) at 75 °C, with sampling (6 μL) at 1, 2, 3, 4, 7, and 10 h intervals. Individual analyte samples were analyzed by HPLC-DAD-ESI(±)MS (Zorbax SB-C_8 column, 150 × 4.6 mm, 5 μm, 1 mL/min gradient elution from 90% H_2O/MeCN to 100% MeCN with 0.05% formic acid as modifier over 15 min) (Figures S6 and S7). Experiment 2: For testing the stability of oxytetracycline (**9**) in simulated gastric acid condition, an aliquot of **9** (100 μg) was treated with 0.01 M HCl (200 μL, pH = 2) at 37 °C, with sampling (6 μL) at 1, 2, 4, 6, 10, and 20 h intervals. Individual analyte samples were analyzed by HPLC-DAD-ESI(±)MS (Zorbax SB-C_8 column, 150 × 4.6 mm, 5 μm, 1 mL/min gradient elution from 90% H_2O/MeCN to 100% MeCN with 0.05% formic acid as modifier over 15 min) (Figure S8). Experiment 3: For testing the stability of viridicatumtoxin A (**1**) under harsher acidic conditions, an aliquot of **1** (0.8 mg) dissolved in 5% (w/v) *p*-TsOH toluene (200 μL) was treated with molecular sieves to remove residual water. The filtered solution was then heated to 100 °C with sampling (5 μL) at 1, 2, 3, 4, 6, 8, 10, 12, 22, 27, 32, and 48 h intervals. Individual analyte samples were dried, redissolved in MeOH, and subjected to HPLC-DAD-ESI(±)MS analysis (Zorbax SB-C8 column, 150 × 4.6 mm column, 5 μm, 1 mL/min gradient elution from 90% H_2O/MeCN to 100% MeCN over 15 min, with constant 0.05% formic acid modifier) (Figure S9).

Purification of Oxytetracycline and Viridicatumtoxin A Acid Degradation Products (11−15). A sample of **9** (150 mg) was dissolved in 0.1 M HCl (1.5 mL) and stirred at 75 °C for 2 h, after which the solution was dried in vacuo to yield a crude product (157.2 mg) that was fractionated by preparative HPLC (Luna C_{18} column, 250 × 21.2 mm, 10 μm, 20 mL/min gradient elution from 90% to 15% H_2O/MeCN over 20 min, with an isocratic 0.01% TFA modifier) to afford anhydro-oxytetracycline (**10**) (t_R = 9.9 min; 8.5 mg, 5.4%), *α*-apo-oxytetracycline (**11**) (t_R = 7.5 min; 36.4 mg, 23.2%), *β*-apo-oxytetracycline (**12**) (t_R = 10.9 min; 12.1 mg, 7.7%), and terrinolide (**13**) (t_R = 12.8 min; 52.1 mg, 33.1%). Note: Anhydro-oxytetracycline (**10**) could not be obtained in pure form as it was unstable to the HPLC acidified mobile phase (0.01% TFA), undergoing facile conversion to **11**−**13**.

A sample of **1** (45 mg) dissolved in 5% (w/v) *p*-TsOH toluene (3 mL) was treated with molecular sieves to remove residual water, and the filtered reaction mixture was heated at 100 °C for 20 h, after which it was dried in vacuo and fractionated by preparative HPLC (Luna C_{18} column, 250 × 21.2 mm, 10 μm, 20 mL/min gradient elution from 35% H_2O/MeCN to 100% MeCN over 20 min, with an isocratic 0.01% TFA modifier) to afford **14** (t_R = 16.7 min; 0.8 mg, 1.8%) and **15** (t_R = 17.7 min; 0.6 mg, 1.3%).

Characterization of Oxytetracycline and Viridicatumtoxin A Acid Degradation Products (11−15). *Oxytetracycline (**9**).* Pale-yellow powder; $[\alpha]_D^{22}$ −119.5 (*c* 0.2, MeOH); UV (MeOH) λ_{max} (log ε) 266 (3.99), 360 (3.86) nm; NMR (600 MHz, DMSO-d_6) see Table S16; ESI(+)MS m/z 461 $[M + H]^+$, ESI(−)MS m/z 459 $[M - H]^-$; HRESI(+)MS m/z 461.1560 $[M + H]^+$ (calcd for $C_{22}H_{25}N_2O_9^+$, 461.1555).

*α-Apo-oxytetracycline (**11**).* Pale-yellow powder; $[\alpha]_D^{22}$ +61.6 (*c* 0.2, MeOH); UV (MeOH) λ_{max} (log ε) 250 (4.53), 332 (3.78), 381 (3.92), 397 (3.93) nm; NMR (600 MHz, DMSO-d_6) see Table S17; ESI(+)MS m/z 443 $[M + H]^+$, ESI(−)MS m/z 441 $[M - H]^-$; HRESI(+)MS m/z 443.1454 $[M + H]^+$ (calcd for $C_{22}H_{23}N_2O_8^+$, 443.1449).

*β-Apo-oxytetracycline (**12**).* Pale-yellow powder; $[\alpha]_D^{22}$ −70.0 (*c* 0.2, MeOH); UV (MeOH) λ_{max} (log ε) 244 (4.46), 332 (3.74), 394 (3.85) nm; NMR (600 MHz, DMSO-d_6) see Table S18; ESI(+)MS m/z 443 $[M + H]^+$, ESI(−)MS m/z 441 $[M - H]^-$; HRESI(+)MS m/z 443.1454 $[M + H]^+$ (calcd for $C_{22}H_{23}N_2O_8^+$, 443.1449).

*Terrinolide (**13**).* Pale-yellow powder; $[\alpha]_D^{22}$ −29.3 (*c* 0.2, MeOH); UV (MeOH) λ_{max} (log ε) 249 (4.53), 332 (3.91), 380 (3.98), 397 (3.98) nm; NMR (600 MHz, DMSO-d_6) see Table S19; ESI(+)MS m/z 398 $[M + H]^+$, ESI(−)MS m/z 396 $[M - H]^-$; HRESI(−)MS m/z 396.0721 $[M - H]^-$ (calcd for $C_{20}H_{14}NO_8^-$, 396.0719).

14. Yellow amorphous powder; $[\alpha]_D^{22}$ +108.0 (*c* 0.04, EtOH); UV (MeOH) λ_{max} (log ε) 251 (4.69), 291 (4.16), 303 (4.22), 394 (4.12) nm; ^{1}H NMR (600 MHz, $CDCl_3$) δ_H 13.03 (1H, s, 12-OH), 10.96 (1H, s, 10-OH), 7.33 (1H, s, H-5), 7.05 (1H, s, H-14), 6.38 (1H, s, H-9), 6.05 (1H, br s, 12a-OH), 5.73 (1H, m, H-17), 3.87 (3H, s, 8-OCH_3), 3.80 (2H, d, *J* = 3.5, H-4), 3.75 (3H, s, 4-$COOCH_3$), 2.26 (2H, m, H-18), 1.91 (1H, dt, *J* = 13.2, 6.2 Hz, H-19*α*), 1.63 (1H, dt, *J* = 13.2, 6.8 Hz, H-19*β*), 1.11 (3H, d, *J* = 1.5 Hz, H-21), 0.87 (3H, s, H-22), 0.85 (3H, s, H-23); ^{13}C NMR (150 MHz, $CDCl_3$) δ_C 191.1 (C-11), 171.5 (C-3), 163.0 (C-10), 162.0 (C-8), 149.4 (C-12), 149.3 (C-6), 144.3 (C-14), 143.4 (C-12a), 132.8 (C-5a), 131.0 (C-16), 126.2 (C-4a), 124.6 (C-7), 124.5 (C-17), 124.4 (C-6a), 117.5 (C-5), 114.7 (C-11a), 106.2 (C-10a), 97.2 (C-9), 68.3 (C-15), 55.8 (8-OCH_3), 52.5 (4-$COOCH_3$), 37.0 (C-20), 35.9 (C-19), 35.9 (C-4), 27.0 (C-23), 26.9 (C-22), 23.2 (C-18), 19.7 (C-21); ESI(+)MS m/z 477 $[M + H]^+$, ESI(−)MS m/z 475 $[M - H]^-$; HRESI(+)MS m/z 477.1911 $[M + H]^+$ (calcd for $C_{28}H_{29}O_7^+$, 477.1908).

15. Yellow amorphous powder; $[\alpha]_D^{22}$ +125.3 (*c* 0.05, EtOH); UV (MeOH) λ_{max} (log ε) 251 (4.74), 292 (4.13), 302 (4.16), 387 (4.15) nm; ^{1}H NMR (600 MHz, $CDCl_3$) δ_H 13.11 (1H, s, 12-OH), 10.92 (1H, s, 10-OH), 7.42 (1H, s, H-5), 7.16 (1H, s, H-14), 6.41 (1H, s, H-9), 5.76 (1H, m, H-17), 3.89 (3H, s, 8-OCH_3), 3.86 (2H, br s, H-4), 2.27 (2H, m, H-18), 1.93 (1H, dt, *J* = 13.3, 6.2 Hz, H-19*α*), 1.62 (1H, dt, *J* = 13.3, 6.7, H-19*β*), 1.12 (3H, d, *J* = 1.5 Hz, H-21), 0.88 (3H, s, H-22), 0.86 (3H, s, H-23); ^{13}C NMR (150 MHz, $CDCl_3$) δ_C 191.2 (C-11), 172.5 (C-3), 163.2 (C-10), 162.2 (C-8), 148.5 (C-6), 147.5 (C-12), 146.5 (C-14), 142.0 (C-12a), 132.7 (C-5a), 130.5 (C-16), 130.2 (C-4a), 129.6 (C-6a), 124.9 (C-17), 124.5 (C-7), 116.6 (C-11a), 111.0 (C-5), 106.1 (C-10a), 97.5 (C-9), 68.5 (C-15), 55.8 (8-OCH_3), 37.1 (C-20), 35.9 (C-19), 33.9 (C-4), 27.0 (C-23), 26.9 (C-22), 23.1 (C-18), 19.7 (C-21); ESI(+)MS m/z 445 $[M + H]^+$, ESI(−)MS m/z 443 $[M - H]^-$; HRESI(−)MS m/z 443.1505 $[M - H]^-$ (calcd for $C_{27}H_{23}O_6^-$, 443.1500).

X-ray Crystallographic Analysis of 1·2MeOH·0.5H_2O. The single crystal of **1**·2MeOH·0.5H_2O was obtained from MeOH by slow evaporation at room temperature. Data were collected at 190 K using an Oxford Diffraction Gemini CCD diffractometer with Cu K*α* radiation, and the crystal was cooled with an Oxford Cryosystems Desktop Cooler. Data reduction was performed with the CrysAllisPro program (Oxford Diffraction version 171.34.40). The structure was solved by direct methods with SHELXS86 and refined with SHELX97.[15] The thermal ellipsoid diagram was produced with ORTEP3,[16] and all calculations were performed within the WinGX package.[17]

$C_{30}H_{31}NO_{10}·2(CH_3OH)·0.5H_2O$, M = 638.65, monoclinic, *a* = 30.1333(7), *b* = 7.7644(2), *c* = 12.9297(3) Å, *V* = 2912.26(12) Å^3, *T* = 190(2) K, space group *C*2, *Z* = 4, 16514 reflections measured, 4539 unique (R_{int} = 0.0413) which were used in all calculations. The final *R*(obs. data) was 0.0466, goodness of fit 1.069. CCDC number 1429664. The absolute structure was confirmed by the methodology of Hooft et al.[18]

■ ASSOCIATED CONTENT

Supporting Information

The Supporting Information is available free of charge on the ACS Publications website at DOI: 10.1021/acs.joc.5b02367.

X-ray crystallography of **1** (CIF)

DOI: 10.1021/acs.joc.5b02367
J. Org. Chem. 2015, 80, 12501−12508

^{1}H and ^{13}C NMR spectra and tabulated 1D and 2D NMR data for **1**−**9**, **11**−**15**, taxonomy of *Paecilomyces* sp., optical rotation study of **1**, acid and heat stability of **1**, **3**, and **9**, HPLC chromatograms, bioassay data (PDF)

AUTHOR INFORMATION

Corresponding Author

*E-mail: r.capon@uq.edu.au.

Notes

The authors declare no competing financial interest.

ACKNOWLEDGMENTS

This research was funded in part by the Institute for Molecular Bioscience, UQ, and the Australian Research Council (DP120100183). Z.S. acknowledges UQ for a Postgraduate Research Scholarship. We acknowledge E. Lacey (BioAustralis) for a sample of viridicatumtoxin A, D. Paterson and H. Zowawi (UQ Centre for Clinical Research) for multidrug-resistant bacteria isolates, X. Xiao (IMB) for advice with synthetic chemistry, and A. Jarrad (IMB) for bioassay support.

REFERENCES

(1) Hutchison, R. D.; Steyn, P. S.; Van Rensburg, S. J. *Toxicol. Appl. Pharmacol.* **1973**, *24*, 507−509.
(2) Zheng, C. J.; Yu, H. E.; Kim, E. H.; Kim, W. G. *J. Antibiot.* **2008**, *61*, 633−637.
(3) Nicolaou, K. C.; Nilewski, C.; Hale, C. R.; Ioannidou, H. A.; ElMarrouni, A.; Koch, L. G. *Angew. Chem., Int. Ed.* **2013**, *52*, 8736−8741.
(4) Nicolaou, K. C.; Hale, C. R.; Nilewski, C.; Ioannidou, H. A.; ElMarrouni, A.; Nilewski, L. G.; Beabout, K.; Wang, T. T.; Shamoo, Y. *J. Am. Chem. Soc.* **2014**, *136*, 12137−12160.
(5) Inokoshi, J.; Nakamura, Y.; Hongbin, Z.; Uchida, R.; Nonaka, K.; Masuma, R.; Tomoda, H. *J. Antibiot.* **2013**, *66*, 37−41.
(6) Chooi, Y. H.; Wang, P.; Fang, J.; Li, Y.; Wu, K.; Wang, P.; Tang, Y. *J. Am. Chem. Soc.* **2012**, *134*, 9428−9437.
(7) Chooi, Y. H.; Hong, Y. J.; Cacho, R. A.; Tantillo, D. J.; Tang, Y. *J. Am. Chem. Soc.* **2013**, *135*, 16805−16808.
(8) Kabuto, C.; Silverton, J. V.; Akiyama, T.; Sankawa, U.; Hutchison, R. D.; Steyn, P. S.; Vleggaar, R. *J. Chem. Soc., Chem. Commun.* **1976**, 728−729.
(9) Silverton, J. V.; Kabuto, C.; Akiyama, T. *Acta Crystallogr., Sect. B: Struct. Crystallogr. Cryst. Chem.* **1982**, *38*, 3032−3037.
(10) De Jesus, A. E.; Hull, W. E.; Steyn, P. S.; van Heerden, F. R.; Vleggaar, R. *J. Chem. Soc., Chem. Commun.* **1982**, 902−904.
(11) Horak, R. M.; Maharaj, V. J.; Marais, S. F.; van Heerden, F. R.; Vleggaar, R. *J. Chem. Soc., Chem. Commun.* **1988**, 1562−1564.
(12) Chooi, Y. H.; Cacho, R.; Tang, Y. *Chem. Biol.* **2010**, *17*, 483−494.
(13) Casy, A. F.; Yasin, A. *Magn. Reson. Chem.* **1985**, *23*, 767−770.
(14) Bendele, A. M.; Carlton, W. W.; Nelson, G. E.; Peterson, R. E.; Grove, M. D. *Toxicol. Lett.* **1984**, *22*, 287−291.
(15) Sheldrick, G. M. *Acta Crystallogr., Sect. A: Found. Crystallogr.* **2008**, *64*, 112−122.
(16) Farrugia, L. J. *J. Appl. Crystallogr.* **1997**, *30*, 565.
(17) Farrugia, L. J. *J. Appl. Crystallogr.* **1999**, *32*, 837−838.
(18) Hooft, R. W.; Straver, L. H.; Spek, A. L. *J. Appl. Crystallogr.* **2008**, *41*, 96−103.

DOI: 10.1021/acs.joc.5b02367
J. Org. Chem. 2015, 80, 12501−12508